Research

Check for updates

Author for correspondence:
Mahendra K. Verma
e-mail: mkv@iitk.ac.in

Boltzmann equation and hydrodynamic equations: their equilibrium and non-equilibrium behaviour

Mahendra K. Verma

Department of Physics, Indian Institute of Technology Kanpur, Kanpur 208016, India

MKV, 0000-0002-3380-4561

This short article summarizes the key features of equilibrium and non-equilibrium aspects of Boltzmann and hydrodynamic equations. Under equilibrium, the Boltzmann equation generates uncorrelated random velocity that corresponds to k^2 energy spectrum for the Euler equation. The latter spectrum is produced using initial configuration with many Fourier modes of equal amplitudes but with random phases. However, for a large-scale vortex as an initial condition, earlier simulations exhibit a combination of $k^{-5/3}$ (in the inertial range) and k^2 (for large wavenumbers) spectra, with the range of k^2 spectrum increasing with time. These simulations demonstrate an approach to equilibrium or thermalization of Euler turbulence. In addition, they also show how initial velocity field plays an important role in determining the behaviour of the Euler equation. In non-equilibrium scenario, both Boltzmann and Navier–Stokes equations produce similar flow behaviour, for example, Kolmogorov's $k^{-5/3}$ spectrum in the inertial range.

This article is part of the theme issue 'Fluid dynamics, soft matter and complex systems: recent results and new methods'.

1. Introduction

This paper, which is based on my talk at the conference *Discrete Simulation of Fluid Dynamics* 2019 (DSFD2019), is a perspective of a fluid dynamist on equilibrium and non-equilibrium features of Boltzmann and hydrodynamic equations. Though this topic has been studied for more than a hundred years, some subtle points are often missed out due to its cross-disciplinary nature. In addition, at present these topics

are being intensely investigated due to a recent surge in interest in *thermalization* of classical and quantum systems [1–4]. Here, I recapitulate only some of the subtle results on the equilibrium and non-equilibrium nature of hydrodynamic systems, along with some new ones.

The Boltzmann equation plays a key role in kinetic theory, and describes the behaviour of a collection of particles [5–10]. This equation forms the basis for non-equilibrium and equilibrium statistical physics. For example, under equilibrium condition, the Boltzmann equation yields Maxwell–Boltzmann distribution for molecules in a microcanonical ensemble [6–9,11].

Hydrodynamics provides another window for the description of systems with a large number of particles. Here, we assume continuum approximation according to which the mean free path length between two collisions of a microscopic particle is much smaller than the system size. Turbulence, a non-equilibrium state of a flow, is often studied in a hydrodynamic picture. Interestingly, many researchers have also studied turbulent flows using the lattice Boltzmann method (LBM) and discrete simulation Monte Carlo (DSMC), which are variants of the Boltzmann equation in discrete space (see [12–17] and references therein). It has been shown that the numerical results of turbulence (flow profiles, energy spectrum, etc.) obtained using hydrodynamic equations, LBM, and DSMC are similar (see, for example, [17,18]). These observations indicate similar *non-equilibrium behaviour* in these diverse descriptions of many-body systems. In recent years, LBM has become a popular numerical scheme for simulating many engineering and natural flows. A major factor in favour of LBM is that they are more amenable to parallelization than many hydrodynamic schemes, especially the spectral method.

Equilibrium behaviour of Boltzmann and hydrodynamic equations has been studied in detail. Under equilibrium, the Boltzmann equation predicts that the velocity of the molecules is uncorrelated in space and time, and they follow the Maxwell–Boltzmann distribution [6–8]. Its equivalent description in hydrodynamics is force-free Euler equation that exhibits a random flow whose energy spectrum is proportional to k^2 [19,20]. This is because each Fourier mode of Euler turbulence has equal energy.

Typically, Euler turbulence is simulated using large flow structures as an initial condition [21–23]. These simulations exhibit a combination of the $k^{-5/3}$ spectrum in the inertial range and k^2 for large wavenumbers [21,22]. With time, the range of the k^2 spectrum increases at the expense of the $k^{-5/3}$ spectrum. Note that the $k^{-5/3}$ spectrum is due to the energy cascade from large scales to intermediate scales, while the k^2 spectrum is due to the equilibrium behaviour at small scales. The above process describes a thermalization scenario for Euler turbulence. Similar thermalization processes have also been studied for Burgers turbulence [24] and for turbulent Bose–Einstein condensate [25].

In this paper, we show that an initial configuration with many Fourier modes of equal amplitude but random phases yield k^2 energy spectrum for all the Fourier modes. This flow is analogous to the random velocity field of the Boltzmann equation. Comparing this result with those by Cichowlas *et al.* [21], we show that initial configuration affects the flow behaviour significantly, and we can generate equilibrium and non-equilbrium behaviour in Euler turbulence for different initial configurations.

Each topic mentioned above—Boltzmann equation, hydrodynamics, LBM, turbulence, equilibrium versus non-equilibrium, thermalization—is very broad. In this short article, we only attempt to contrast the equilibrium and non-equilibrium behaviour of Boltzmann and hydrodynamic equations. More specifically, we highlight thermalization, and discuss how we can obtain equilibrium or non-equilibrium behaviour depending on the choice of initial configuration.

The outline of the paper is as follows. In §2, we briefly introduce Boltzmann and hydrodynamic equations. In §§ 3 and 4, we describe the key equilibrium and non-equilibrium features of these equations. We conclude in §5.

2. Brief introduction to Boltzmann and hydrodynamic equations

In statistical physics, we deal with a large number of atoms or molecules. Let us consider N molecules of the same species that are specified by their position (**r**) and velocity (**u**). In classical

mechanics, it is customary to describe the dynamics of this collection in $6N$-dimensional phase space whose coordinates are $(x_a, y_a, z_a, p_{x,a}, p_{y,a}, p_{z,a})$, where a is the molecule label, and $x_a, p_{x,a}$ are, respectively, the x components of the position and momentum of ath molecule [26]. A point in the phase space provides a unique representation of a state of the above mechanical system.

For large N, it is impractical to work in phase space due to its enormous dimensionality. Instead, the above system is represented as N points in a six-dimensional μ-space whose coordinates are (x, y, z, p_x, p_y, p_z). The density of the μ-space points at point $(\mathbf{r}, \mathbf{u})$ and at time t is denoted by $f(\mathbf{r}, \mathbf{u}, t)$, called the *distribution function* [5–10]. Boltzmann [5] derived the following equation, called the *Boltzmann equation*, to describe the evolution of $f(\mathbf{r}, u, t)$:

$$\frac{\partial f}{\partial t} + \dot{\mathbf{r}} \cdot \nabla f + \dot{\mathbf{u}} \cdot \nabla_\mathbf{u} f = \left(\frac{\partial f}{\partial t} \right)_{\text{coll}}, \tag{2.1}$$

where $(\partial f / \partial t)_{\text{coll}}$, the collision term, is typically computed for the collisions between two molecules. If the two molecules have incoming velocities $\mathbf{u}_1$ and $\mathbf{u}_2$, and outgoing velocities $\mathbf{u}'_1$ and $\mathbf{u}'_2$, then it can be shown that [5,6,8,9]

$$\left(\frac{\partial f}{\partial t} \right)_{\text{coll}} = \int d^3 p_2 \, d\Omega \, |\mathbf{u}_1 - \mathbf{u}_2| \frac{d\sigma}{d\Omega} (f'_1 f'_2 - f_1 f_2), \tag{2.2}$$

where $d\sigma / d\Omega$ is the differential cross section, and

$$f_1 = f(\mathbf{r}, \mathbf{u}_1, t); \quad f_2 = f(\mathbf{r}, \mathbf{u}_2, t) \tag{2.3}$$

and

$$f'_1 = f(\mathbf{r}, \mathbf{u}'_1, t); \quad f'_2 = f(\mathbf{r}, \mathbf{u}'_2, t). \tag{2.4}$$

The above derivation assumes *molecular chaos*, according to which the velocities of the colliding particles are uncorrelated and independent of their position. In the subsequent discussion, we will discuss the equilibrium solution of the Boltzmann equation. Note that kinetic theory forms a basis for many works of statistical physics, and it successfully describes many macroscopic phenomena, for example, thermodynamics, transport processes and hydrodynamics.

It is much more convenient to work in real space with only $\mathbf{r}$ as an independent variable. Here, the relevant variables are the density field (ρ) and velocity field ($\mathbf{u}$). Under hydrodynamic approximation, it is assumed that the smallest length of hydrodynamics is much larger than the collisional mean free path length. By employing conservation of mass and linear momentum under collisions, one can derive the following equations [7,8,10]:

$$\frac{\partial \rho}{\partial t} + \nabla \cdot (\rho \mathbf{u}) = 0 \tag{2.5}$$

and

$$\rho \left[\frac{\partial \mathbf{u}}{\partial t} + (\mathbf{u} \cdot \nabla) \mathbf{u} \right] = -\nabla p + \eta \nabla^2 \mathbf{u} + (\zeta + \eta/2) \nabla (\nabla \cdot \mathbf{u}) + \mathbf{F}_u, \tag{2.6}$$

where p is the pressure field, $\mathbf{F}_u$ is the external force field, and η and ζ are the viscous parameters. The above equations are the continuity and Navier–Stokes equations, respectively. In this paper, we focus on incompressible flows for which $\nabla \cdot \mathbf{u} = 0$. Also note that η and ζ vanish for the Euler equation, and $\mathbf{F}_u = 0$ for the force-free case.

In the next two sections, we consider some generic equilibrium and non-equilibrium behaviour of the Boltzmann equation and its hydrodynamic counterpart.

3. Equilibrium behaviour

Thermodynamics and equilibrium statistical physics deal with systems under equilibrium. Using kinetic theory, Boltzmann showed that the distribution function for an equilibrium configuration is Gaussian in u [5,6,8,9]. The arguments are as follows. For simplicity, we assume that the system

is made of one kind of molecule. For a homogeneous, isotropic, steady, and force-free ($\mathbf{F}_u = 0$) system, the left-hand side of equation (2.1) vanishes. Therefore, $(\partial f/\partial t)_{\text{coll}} = 0$, and hence

$$f_1' f_2' = f_1 f_2, \tag{3.1}$$

one of whose trivial homogeneous and isotropic solutions is [7,8,10]

$$f(u) = \left(\frac{m}{2\pi k_B T}\right)^{3/2} \exp\left(-\frac{mu^2}{2k_B T}\right), \tag{3.2}$$

where m is the mass of the molecules, k_B is Boltzmann constant, and T is the temperature of the system. On average, each molecule has an equal kinetic energy: $m\langle u^2\rangle/2 = k_B T$. The velocities of the molecules are uncorrelated with each other. In addition, the energy exchange among the molecules satisfies a detailed balance condition. That is, on average, a molecule neither receives nor gives energy to another molecule.

In hydrodynamic descriptions, the Euler equation, which has $\nu = 0$, exhibits equilibrium behaviour under certain conditions [27]. Under equilibrium, the real-space velocity field (at equal time) is uncorrelated, i.e.

$$\langle u_i(\mathbf{r}, t) u_j(\mathbf{r}', t)\rangle = \langle u^2\rangle \delta_{ij}\delta(\mathbf{r} - \mathbf{r}'). \tag{3.3}$$

Here, $\mathbf{u}(\mathbf{r}, t)$ is interpreted as the average velocity of many molecules in a small region near the point $\mathbf{r}$ and at time t. Using the Wiener–Khinchin theorem, we deduce that the modal kinetic energy

$$C(\mathbf{k}) = \frac{1}{2}\langle|\mathbf{u}(\mathbf{k})|^2\rangle = \frac{E}{N}, \tag{3.4}$$

where E is the total energy of the system that is evenly distributed across N available Fourier modes. The above spectrum represents white noise. If Fourier modes reside in a wavenumber sphere of radius of k_{max}, then, in three-dimensional (3D) space,

$$N = \frac{4}{3}\pi k_{\text{max}}^3. \tag{3.5}$$

For the above system, called the *truncated Euler equation*, the shell spectrum is [20]

$$E(k) = \frac{3E}{k_{\text{max}}^3}k^2. \tag{3.6}$$

For two-dimensional (2D) hydrodynamics, the corresponding shell spectrum is

$$E(k) = \frac{2E}{k_{\text{max}}^2}k \tag{3.7}$$

and

$$N = \pi k_{\text{max}}^2. \tag{3.8}$$

The above relations were first derived by Lee [19] and Kraichnan [20] using Liouville's theorem and ergodic hypothesis. The above energy spectra get altered in the presence of kinetic helicity in 3D or enstrophy in 2D [20], but this discussion is beyond the scope of this paper.

In kinetic theory, the mean free path length is the only relevant length scale (apart from trivial molecular size). The corresponding hydrodynamic equation, the Euler equation, has a range of wavenumbers (up to k_{max}). This is because generation of an *ideal* random uncorrelated signal of equation (3.3) requires an infinite number of Fourier modes. Note, however, that the velocity field becomes correlated at the scale of molecular size, denoted by b. Therefore, equation (3.3) could be replaced by

$$\langle u_i(\mathbf{r}, t) u_j(\mathbf{r}', t)\rangle = \langle u^2\rangle \delta_{ij}\frac{1}{b}\theta(b - |\mathbf{r} - \mathbf{r}'|), \tag{3.9}$$

where $\theta(\cdot)$ is the step function. The above definition provides an estimate of the wavenumber cut-off k_{max} as $1/b$.

In the Fourier-space version of the Euler equation, the energy transfer from a Fourier mode to another Fourier mode vanishes statistically. It follows from the mode-to-mode energy transfer formula [28,29]:

$$S^{uu}(\mathbf{k}|\mathbf{p}|\mathbf{q}) = \Im[\{\mathbf{k} \cdot \mathbf{u}(\mathbf{q})\}\{\mathbf{u}(\mathbf{p}) \cdot \mathbf{u}^*(\mathbf{k})\}], \tag{3.10}$$

which is the energy transfer from mode $\mathbf{u}(\mathbf{p})$ to mode $\mathbf{u}(\mathbf{k}')$ with the mediation of mode $\mathbf{u}(\mathbf{q})$. Verma [30] computed the above quantity using field-theory and showed that for non-helical flows, ensemble average of $S^{uu}(\mathbf{k}|\mathbf{p}|\mathbf{q})$ is

$$\langle S^{uu}(\mathbf{k}|\mathbf{p}|\mathbf{q})\rangle = \frac{1}{\mathrm{denr}}[k'\sin(\beta-\gamma)C(\mathbf{p})C(\mathbf{q}) + p\sin(\gamma-\alpha)C(\mathbf{k}')C(\mathbf{q})$$
$$+ q\sin(\alpha-\beta)C(\mathbf{k}')C(\mathbf{p}) + k'\sin\beta C(\mathbf{q})\{C(\mathbf{k}') - C(\mathbf{p})\}], \tag{3.11}$$

where

$$\mathrm{denr} = \nu(k)k^2 + \nu(p)p^2 + \nu(q)q^2, \tag{3.12}$$

and α, β, γ are the respective internal angles across k, p, q in a triangle formed by vectors $(\mathbf{k}, \mathbf{p}, \mathbf{q})$. In equation (3.11), we substitute $C(\mathbf{k})$ of equation (3.4), and employ the following identity:

$$\frac{\sin\alpha}{k} = \frac{\sin\beta}{p} = \frac{\sin\gamma}{q}, \tag{3.13}$$

that yields

$$\langle S^{uu}(\mathbf{k}|\mathbf{p}|\mathbf{q})\rangle = 0. \tag{3.14}$$

Thus we verify detailed balance of energy transfer for the equilibrium configuration of the Euler equation.

We performed a numerical simulation to test the aforementioned equilibrium behaviour of the Euler equation. For the same, we simulated a force-free incompressible Euler equation on a 128^3 grid using pseudospectral code TARANG [31,32]. We imposed periodic boundary conditions on all the walls. Importantly, for the initial condition, we took the amplitudes of all the Fourier modes to be a constant $(E/N = 10^{-5})$, and set their phases as random. In particular, we chose [30]

$$\mathbf{u}(\mathbf{k}) = A\exp(i\phi(\mathbf{k}))\hat{e}_2(\mathbf{k}), \tag{3.15}$$

where $\hat{e}_2$ is the component of the velocity field in the Craya–Herring basis [30], and the phase $\phi(\mathbf{k})$ is a random variable taken from a uniform distribution in the range $[0, 2\pi]$. The above choice ensures zero kinetic helicity for the flow. The above initial condition is chosen so as to nullify the energy transfers across scales during the initial phase itself (see equation (3.14)).

The flow is evolved until $t = 1$ in the unit of L/U, where L, U are the large-scale length and velocity, respectively. In figure 1, we plot the energy spectrum $E(k)$ for the final flow profile. Clearly, $E(k) \sim k^2$, consistent with equation (3.6) for flows in equilibrium. As shown above, $\langle S(\mathbf{k}|\mathbf{p}|\mathbf{q})\rangle = 0$ for $E(k) \sim k^2$. Thus, we deduce that the energy transfers among modes remain zero during the evolution, thus respecting the detailed balance of energy transfer. Interestingly, for the random velocity field, the nonlinear term in Euler turbulence yields zero energy transfer among any pair of modes, leading to equilibrium behaviour. This is an example of a nonlinear system that yields random behaviour. Contrast this with a view that nonlinear interactions typically induce order out of chaos, as proposed by Prigogine [33,34].

There have been earlier numerical simulations that attempted to verify the above energy spectrum [21,35,36]. In most of these simulations, small wavenumber Fourier modes were excited as the initial condition. For example, Cichowlas *et al.* [21] simulated Euler turbulence on $256^2, 512^3, 1024^3, 1600^3$ grids with initial condition as

$$\mathbf{u}(\mathbf{r}, t = 0) = \hat{x}\sin x\cos y\cos z - \hat{y}\cos x\sin y\cos z, \tag{3.16}$$

which is a Taylor–Green vortex, whose extent is the box size. They observed that for the developed flow, the energy spectrum $E(k)$ is a combination of Kolmogorov's $k^{-5/3}$ spectrum at intermediate wavenumbers, and k^2 at large wavenumbers. See figure 2 for an illustration.

6

royalsocietypublishing.org/journal/rsta   *Phil. Trans. R. Soc. A* **378**: 20190470
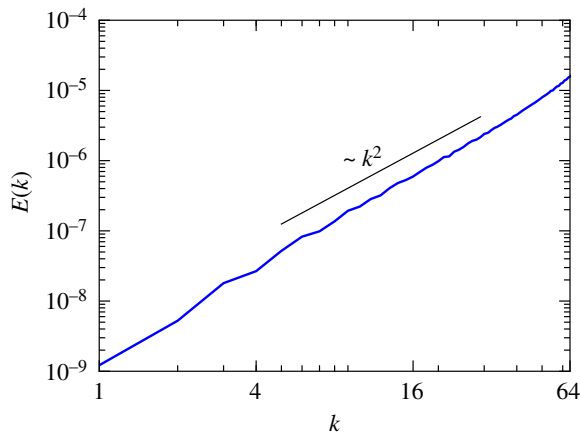
Figure 1. For a spectral simulation of force-free Euler equation, the energy spectrum $E(k) \sim k^2$ at $t = 1$ in non-dimensional time unit. (Online version in colour.)

| non equilibrium | equilibrium |
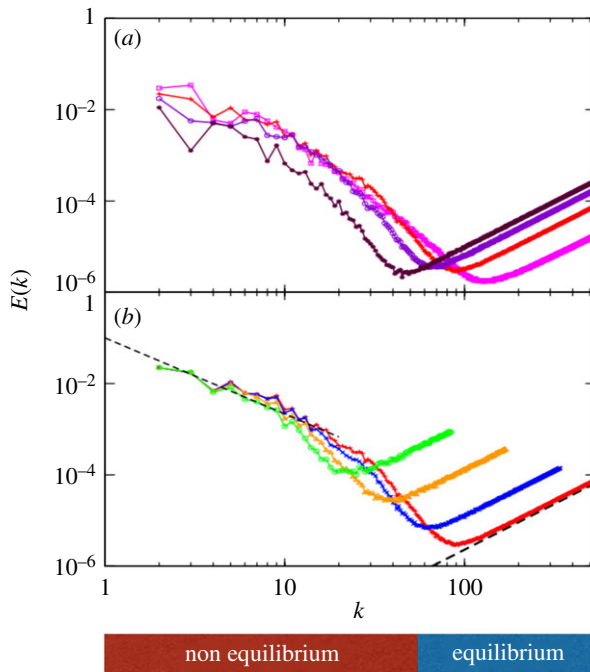
Figure 2. (*a*) For a Euler turbulence simulation on a 1600^3 grid, the energy spectrum at $t = 6.5, 8, 10, 14$ in non-dimensional time units (pink, orange, purple and brown curves, respectively; or in increasing amplitudes at large wavenumbers). (*b*) The energy spectra for $256^2, 512^3, 1024^3, 1600^3$ grids at $t = 8$ (green, yellow, blue and red curves, respectively; or in decreasing amplitudes at large wavenumbers). From Cichowlas *et al.* [21]. Reproduced with permission from APS. (Online version in colour.)

In the flow generated in the simulations of Cichowlas *et al.* [21], due to the dominance of large scales, the kinetic energy cascades to intermediate scales, and then to small scales. It can be shown that for the Euler equation, the energy flux for a wavenumber sphere of radius k_0 is given by

$$\Pi(k_0, t) = -\frac{\mathrm{d}}{\mathrm{d}t} \int_0^{k_0} \mathrm{d}k E(k, t). \tag{3.17}$$

Because of the loss of energy in the sphere, the flux $\Pi(k_0, t)$ is positive. Consequently, the interacting modes are not in equilibrium. After some time, the intermediate scales exhibit the Kolmogorov's $k^{-5/3}$ spectrum. However, the Fourier modes at small scales are in equilibrium, hence $E(k) \sim k^2$ for these scales. As time progresses, the k^2 regime increases at the expense of the $k^{-5/3}$ regime (figure 2a). We expect an asymptotic k^2 spectrum that represents the *asymptotic equilibrium state*. Thus, the above numerical results of Cichowlas *et al.* [21] describe the *approach to equilibrium* in Euler turbulence. We remark that the existence of energy flux breaks the detailed balance of energy transfer for the modes in the intermediate range. The energy flux vanishes asymptotically as we approach the equilibrium state. Interestingly, the above description is in terms of energy flux, not entropy, which is often employed in non-equilibrium statistical physics.

The above example demonstrates the strong effects of initial configuration on the behaviour of Euler turbulence. Our k^2 spectrum and the mixed spectrum ($k^{-5/3}$ and k^2) of Cichowlas *et al.* [21] differ primarily due to the choice of initial velocity configuration. Random initial velocity configuration with equal amplitudes for all the Fourier modes yields a k^2 spectrum without any energy flux, but initial configuration with large-scale velocity field yields a mixed energy spectrum. The later flow is more ordered and is in a non-equilibrium state, and it evolves towards the equilibrium configuration with asymptotic k^2 spectrum.

It is important to note that the Kolmogorov flow, in which forcing is employed at intermediate scales, also exhibits $E(k) \sim k^2$ for wavenumbers smaller than the forcing wavenumbers [35,36]; it is believed that the small wavenumber modes are in equilibrium. It is an interesting example in which the large-scale structures are in equilibrium, while the inertial and small-scale modes are not in equilibrium.

In the next section, we will describe the non-equilibrium behaviour of Boltzmann and Navier–Stokes equations.

4. Non-equilibrium behaviour

On an introduction of viscosity, hydrodynamic systems exhibit non-equilibrium behaviour. Some of the leading examples of such flows are hydrodynamic turbulence, turbulent thermal convection, magnetohydrodynamic turbulence, etc. [23,27]. In such systems, the fluid is typically forced at large scales, while the viscous force destroys the fluid kinetic energy at small scales [23, 27,37]. Note that the scale separation between the energy injection wavenumber and dissipation wavenumber induces a kinetic energy flux that breaks the detailed balance. Therefore, the above turbulent systems are far from equilibrium. In the following discussion we contrast the equilibrium and non-equilibrium behaviour of hydrodynamic turbulence using energy spectrum, energy flux and velocity correlations as diagnostics.

Hydrodynamic turbulence exhibits a constant energy flux and $k^{-5/3}$ energy spectrum in the inertial range, i.e. [23,27,37]

$$\Pi(k) = \text{const} = \epsilon_u \tag{4.1}$$

and

$$E(k) = K_{\text{Ko}} \epsilon_u^{2/3} k^{-5/3}, \tag{4.2}$$

where ϵ_u is the energy dissipation rate.[1] Consequently, the velocity field of a turbulent flow exhibits nonzero correlation, in contrast to equation (3.3) for the equilibrium case. It can be easily shown that [23,27,37]

$$\langle \mathbf{u}(\mathbf{r}) \cdot \mathbf{u}(\mathbf{r} + \mathbf{l}) \rangle = \langle u^2 \rangle - C(\epsilon_u l)^{2/3}, \tag{4.3}$$

where C is a constant. Also, in a turbulent flow, the distance between two nearby particles increases with time as $t^{3/2}$ (called Taylor diffusion) [38], in strong contrast to the corresponding variation as $\sqrt{t}$ for the equilibrium case [8]. In addition, we can determine the arrow of time in turbulent systems using energy flux [39,40], while time is frozen in equilibrium systems. The particle trajectories also provide a measure of irreversibility or non-equilibrium nature of

---

[1]Contrast this with equilibrium hydrodynamics that exhibits $\Pi(k) = \epsilon_u = 0$ and $E(k) \sim k^2$.

the flow [41–43]. Note that in the dissipation range of the Navier–Stokes equation, the energy spectrum is exponential in k. Pao [44] argued the inertial-dissipation energy spectrum to be of the form $k^{-5/3} \exp(-(k/k_d)^{4/3})$, where k_d is Kolmogorov's wavenumber; Verma *et al.* [45] verified this scaling using numerical simulation. The energy transferred to the microscopic scales heats up the molecules. Hence, we can argue that the microscopic part of the system is in quasi-equilibrium due to slow heating. Contrast the disipative spectrum $k^{-5/3} \exp(-(k/k_d)^{4/3})$ with the k^2 spectrum for large k's of Euler turbulence [21].

The aforementioned non-equilibrium behaviour of fluid flows has been observed in many experiments and numerical simulations of hydrodynamics. Due to its high accuracy, the pseudospectral method [46] is often employed for testing Kolmogorov's theory of turbulence. Refer to [23,27], and references therein for numerous hydrodynamic results. Since the present paper is part of the proceedings of the conference on *Discrete Simulations of Fluid Dynamics*, I describe some of the recent discrete simulations that reproduce Kolmogorov's $k^{-5/3}$ energy spectrum. In general, LBM implementations are second-order accurate, but their accuracy can be improved using advanced algorithms, as in finite-difference schemes [14].

Though there are many methods to simulate particles in kinetic theory, here we present some of the recent results that employ Direct Simulation Monte Carlo (DSMC) [16], and LBM [12,14]. Gallis *et al.* [17] simulated three-dimensional turbulence using DSMC and spectral element methods. For the initial condition, they used a large-scale Taylor–Green vortex of equation (3.16). They reported a close agreement between the DSMC and spectral results. For example, they obtained Kolmogorov's $k^{-5/3}$ energy spectrum in both the methods. At the final time, the flow profiles of the two runs are very similar.

In LBM, the Bhatnagar–Gross–Krook (BGK) procedure is adopted to obtain local equilibrium in the flow [12–15]. Many numerical simulations demonstrate that both hydrodynamic simulations and LBM simulations yield similar results, for example, $k^{-5/3}$ spectrum for 3D hydrodynamic turbulence (see [12–15,17,18] and references therein). Martinez *et al.* [18] performed fluid simulations of 2D hydrodynamic turbulence using LBM and spectral method in a periodic box of size $(2\pi)^2$, and compared the results in detail. They used a 512^2 grid for LBM and a 256^2 grid for the spectral simulation. For the initial condition, they employed two sharp vortices of opposite signs. The Reynolds number of the flow based on the relaxation parameter was 10000. They observed remarkable similarities between the LBM and spectral results, thus illustrating functional equivalence of the two methods.

The discrete methods are less accurate compared to the pseudo-spectral scheme. Still, given sufficiently large lattice, discrete methods capture the essential non-equilibrium features of turbulence. This is due to fact that the presence of large-scale structures and small-scale dissipation naturally generates the energy cascade, and hence Kolmogorov's $k^{-5/3}$ spectrum. Thus, inaccurate methods too capture this *robust* feature. Note, however, that discrete methods require larger grids than the spectral method due to the lower accuracy of discrete methods.

It is important to note that numerical implementations of LBM and DSMC have distinct benefits over their hydrodynamic counterparts [12–15,47,48]. For example, computer programs based on LBM and DSMC can be efficiently parallelized; they can also take advantage of a large number of cores available in graphical processing units (GPUs). In addition, implementation of complex boundary conditions is easier in LBM than in a spectral method [14,15,32]. As a result, LBM is often employed to simulate numerous complex engineering flows, e.g. flows around automobiles, cooling of computer CPU, etc. [14,15]. This extensive and important topic however is beyond the scope of this paper.

In Kolmogorov flows where the forcing is employed at the intermediate scales, the spectrum beyond the forcing band is similar to that in hydrodynamic turbulence [35,36]. That is, we obtain $k^{-5/3}$ spectrum in the inertial range, and an exponential tail in the dissipative range. As described in the last section, the small wavenumber modes exhibit k^2 spectrum for Kolmogorov flows.

We conclude in the next section.
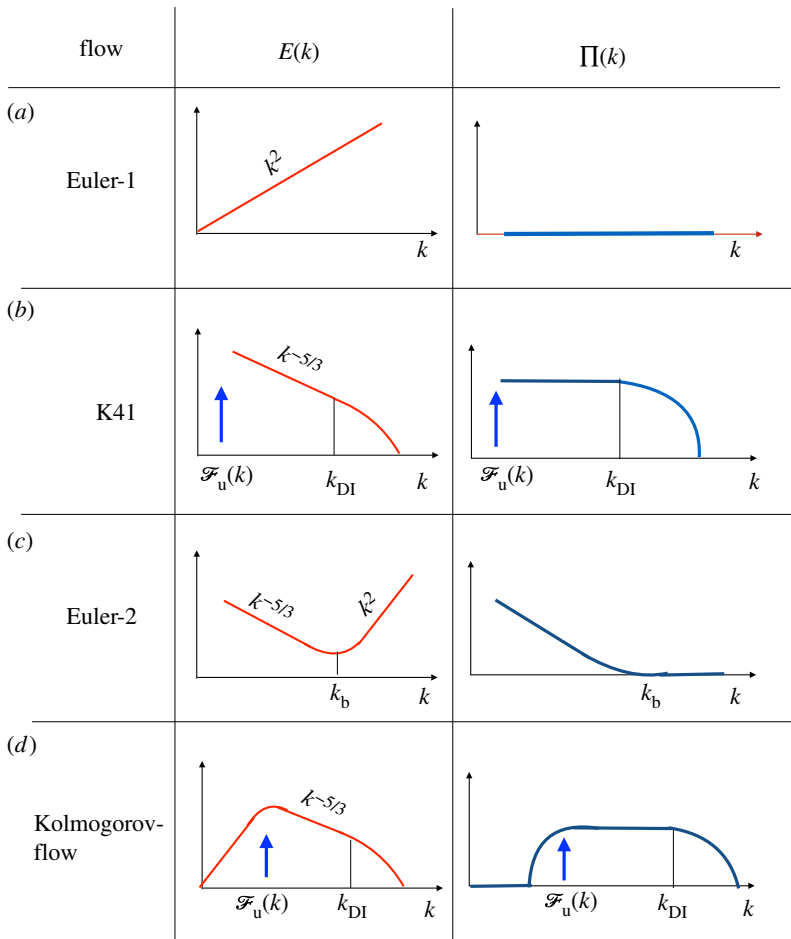
Figure 3. Schematic energy spectra and fluxes for various kinds of flows (*a*) Euler-1: unforced Euler flow that has random uncorrelated initial configuration (white noise). (*b*) K41: turbulent flow of Kolmogorov [37] model. Such flows have small viscosity, and they are forced at large scales. (*c*) Euler-2: unforced Euler flow whose initial condition is large-scale Taylor–Green vortex. (*d*) Kolmogorov-flow: flow that is forced at an intermediate scale. (Online version in colour.)

5. Summary and discussions

In this paper, we reviewed some of the important equilibrium and non-equilibrium properties of Boltzmann and hydrodynamic equations. Boltzmann, Gibbs, and others demonstrated that the particle velocity under equilibrium configuration is given by Maxwell–Boltzmann distribution, and that the total energy of the system is equipartitioned among all the particles [5]. Interestingly, similar behaviour is observed in the force-free Euler equation for a random initial configuration; such systems exhibit steady equilibrium behaviour with energy spectrum of k^2 [19,20]. Thus, both Boltzmann and hydrodynamic equations exhibit equilibrium behaviour for a random initial condition. We illustrate schematic energy spectrum and flux for such flows in figure 3*a*.

In the presence of viscosity, the Navier–Stokes equation (hydrodynamic description) exhibits non-equilibrium behaviour. According to Kolmogorov's famous theory of forced hydrodynamic turbulence, the energy injected at large scales is transferred to the intermediate scales, and then to small scales. The steady-state energy spectrum in the inertial range is proportional to $k^{-5/3}$, while that in the dissipation range is of the form $k^{-5/3} \exp(-(k/k_d)^{4/3})$. See figure 3*b* for an illustration. The large-scale forcing and initial configuration, as well as the viscous dissipation at small scales,

play a crucial role in the above behaviour. Decaying turbulence with large-scale structures also exhibits $k^{-5/3}$ spectrum in the inertial range. Interestingly, the above features have also been observed in kinetic theory, mainly LBM [12–15] and discrete simulation Monte Carlo (DSMC) [17]. Note that Boltzmann's equation is derived using microscopic dynamics. Still, the coarse-grained solution of Boltzmann's equation exhibits turbulence properties under appropriate conditions.

In the force-free Euler equation, which has no external force and viscosity, an initial excitation at large scales yields a combination of Kolmogorov's $k^{-5/3}$ spectrum in the intermediate range and k^2 spectrum in the dissipative range, as illustrated in figure 3c. The $k^{-5/3}$ spectrum is due to the energy transfer from large scales to intermediate scales, while the k^2 spectrum at small scales is attributed to the equilibrium behaviour at these scales. With time, the range of k^2 spectrum increases at the expense of the $k^{-5/3}$ regime. This process illustrates thermalization of Euler turbulence in terms of energy flux and spectrum, rather than entropy. Based on the above observations, we expect that the Boltzmann equation without dissipation to yield a similar steady state. Note however that most of the LBM simulations involve a finite dissipation. Also, a decaying turbulence with random initial velocity at all scales may exhibit a k^2 spectrum.

The above observations indicate that initial configuration plays a major role in determining system's behaviour. A noisy initial excitation at all scales is expected to yield equilibrium behaviour [11]. However, initial excitation at large scales yield non-equilibrium behaviour. Thus, the energy transfers across various scales play a major role in creating a non-equilibrium behaviour. It may be interesting to relate these fluxes to the entropy production mechanism and irreversibility proposed by Prigogine [33,34]. External forcing too plays an important role in setting equilibrium or non-equilibrium behaviour in flows. For example, forcing at large scales sets up non-equilibrium energy cascade prescribed in Kolmogorov's theory of turbulence. However, forcing at an intermediate scale, say near $k = k_f$ as in Kolmogorov flow, yields k^2 spectrum for $k < k_f$, and a combination of $k^{-5/3}$ and exponential spectrum for $k > k_f$. See figure 3d for an illustration. Also, various forms of random forcing are expected to yield different energy spectra [49].

The results on Euler turbulence provide several interesting insights into the thermalization process. They demonstrate the importance of initial condition for the thermalization process. In addition, these results also indicate that energy transfers or energy flux could be a good diagnostics for understanding thermalization in other setups, for example, quantum systems [2–4].

Though numerical simulations using LBM and hydrodynamic methods exhibit similar behaviour, it is not certain if some of the analytical hydrodynamic laws could be derived using the Boltzmann equation alone. Kolmogorov [37] derived the four-fifth law of turbulence starting from Navier–Stokes equations under the assumption of large-scale forcing and small viscosity. Also, the nonlinear term generates energy cascade from the large scales to intermediate scales, and then to the viscous scales.

Although Navier–Stokes equations can be derived from the Boltzmann equation, it is still very cumbersome, if not impossible, to derive the energy flux in the framework of kinetic theory. The energy flux is a multi-scale energy transfer, and it is difficult to formulate it using the microscopic viewpoint alone. Note however that the coarse-grained velocity field can be computed by averaging over particle velocities of lattice-Boltzmann simulation. Gallis et al. [17] computed the energy spectrum of the flow using this procedure. However, the $k^{-5/3}$ spectrum reported by Gallis et al. is based on post-processing; it is not the same as deriving Kolmogorov's four-fifth law from the first principle.

The above phenomenon is analogous to the theory of phase transition proposed by Landau and Wilson [50]. Some spin systems exhibit paramagnetic to ferromagnetic transition on decrease of temperature. So far, such phase transition has not been derived analytically for three-dimensional Ising spins. However, Wilson [51] constructed the free energy of the system using coarse-grained magnetization, and successfully demonstrated the existence of paramagnetic to ferromagnetic phase transition. Here, Ising spins form microscopic description (analogous to kinetic theory), while coarse-grained magnetization is the macroscopic description, similar to

fluid picture of the Navier–Stokes equation. This example also demonstrates that macroscopic descriptions reveal certain natural laws that are very difficult to derive using microscopic theory alone.

In a similar manner, it will be very cumbersome to derive Taylor's diffusion using kinetic theory, but it is straightforward to do so using Kolmogorov's theory of turbulence. Verma [52,53] argues that the structures in nature, as well as their laws, are organized hierarchically. In this framework, kinetic theory (or Boltzmann's equation) describes dynamics at microscopic scales, while hydrodynamic equations are useful for describing phenomena at a coarser level. Description of flows at planetary and galactic scales requires even further coarse-grained pictures. This hierarchical prescription tends to resolve some of the aforementioned difficulties.

In summary, both Boltzmann and hydrodynamic equations capture multiscale features of turbulent flows. These methods have their own practical advantages that become handy for simulating engineering and natural flows.

References

1. Hinrichsen H, Gogolin C, Janotta P. 2011 Non-equilibrium dynamics, thermalization and entropy production. *J. Phys.: Conf. Ser.* **297**, 012011. (doi:10.1088/1742-6596/297/1/012011)
2. Langen T, Geiger R, Schmiedmayer J. 2015 Ultracold atoms out of equilibrium. *Annu. Rev. Condens. Matter Phys.* **6**, 201–217. (doi:10.1146/annurev-conmatphys-031214-014548)
3. Deutsch JM. 2018 Eigenstate thermalization hypothesis. *Rep. Prog. Phys.* **81**, 082001–17. (doi:10.1088/1361-6633/aac9f1)
4. Wilming H, Goihl M, Roth I, Eisert J. 2019 Entanglement-ergodic quantum systems equilibrate exponentially well. *Phys. Rev. Lett.* **123**, 200604. (doi:10.1103/PhysRevLett.123.200604)
5. Boltzmann L. 2003 Further studies on the thermal equilibrium of gas molecules. In *The kinetic theory of gases: an anthology of classic papers with historical commentary*, pp. 262–349. Singapore: World Scientific.
6. Liboff RL. 1998 *Kinetic theory*. New York, NY: Wiley.
7. Choudhuri AR. 1998 *The physics of fluids and plasmas: an introduction for astrophysicists*. Cambridge, UK: Cambridge University Press.
8. Huang K. 2008 *Statistical mechanics*. 2nd edn: New York, NY: John Wiley & Sons.
9. Lifshitz EM, Pitaevskii LP. 2012 *Physical kinetics*. Course of Theoretical Physics. Oxford, UK: Pergamon Press.
10. Siscoe GL. 1983 Solar system magnetohydrodynamics. In *Solar terrestrial physics principles and theoretical foundations* (ed. RL Carovillano, JM Forbes). Dordrecht, The Netherlands: D. Reidel Publishing Company.
11. Landau LD, Lifshitz EM. 1980 *Statistical physics*, 3rd edn. Course of Theoretical Physics. Oxford, UK: Elsevier.
12. Benzi R, Succi S, Vergassola M. 1992 The lattice Boltzmann equation: theory and applications. *Phys. Rep.* **222**, 145–197. (doi:10.1016/0370-1573(92)90090-M)
13. Chen S, Doolen GD. 1998 Lattice Boltzmann method for fluid flows. *Annu. Rev. Fluid Mech.* **30**, 329–364. (doi:10.1146/annurev.fluid.30.1.329)
14. Succi S. 2001 *The lattice Boltzmann equation for fluid dynamics and beyond*. Oxford, UK: Clarendon Press.
15. Aidun CK, Clausen JR. 2010 Lattice-Boltzmann method for complex flows. *Annu. Rev. Fluid Mech.* **42**, 439–472. (doi:10.1146/annurev-fluid-121108-145519)
16. Bird GA. 1994 *Molecular gas dynamics and the direct simulation of gas flows*. Oxford, UK: Claredon.

17. Gallis MA, Bitter NP, Koehler TP, Torczynski JR, Plimpton SJ, Papadakis G. 2017 Molecular-level simulations of turbulence and its decay. *Phys. Rev. Lett.* **118**, 064501. (doi:10.1103/PhysRevLett.118.064501)

18. Martinez DO, Matthaeus WH, Chen S, Montgomery DC. 1994 Comparison of spectral method and lattice Boltzmann simulations of two-dimensional hydrodynamics. *Phys. Fluids* **6**, 1285–1298. (doi:10.1063/1.868296)

19. Lee TD. 1952 On some statistical properties of hydrodynamical and magneto-hydrodynamical fields. *Quart. Appl. Math.* **10**, 69–74. (doi:10.1090/qam/51081)

20. Kraichnan RH. 1973 Helical turbulence and absolute equilibrium. *J. Fluid Mech.* **59**, 745–752. (doi:10.1017/S0022112073001837)

21. Cichowlas C, Bonaïti P, Debbasch F, Brachet ME. 2005 Effective dissipation and turbulence in spectrally truncated Euler flows. *Phys. Rev. Lett.* **95**, 264502. (doi:10.1103/PhysRevLett.95.264502)

22. Krstulovic G, Mininni PD, Brachet ME, Pouquet AG. 2009 Cascades, thermalization, and eddy viscosity in helical Galerkin truncated Euler flows. *Phys. Rev. E* **79**, 056304. (doi:10.1103/PhysRevE.79.056304)

23. Frisch U. 1995 *Turbulence: the legacy of A. N. Kolmogorov*. Cambridge, UK: Cambridge University Press.

24. Frisch U, Kurien S, Pandit R, Pauls W, Ray SS, Wirth A, Zhu JZ. 2008 Hyperviscosity, galerkin truncation, and bottlenecks in turbulence. *Phys. Rev. Lett.* **101**, 144501. (doi:10.1103/PhysRevLett.101.144501)

25. Krstulovic G, Brachet ME. 2011 Dispersive bottleneck delaying thermalization of turbulent Bose-Einstein condensates. *Phys. Rev. Lett.* **106**, 115303. (doi:10.1103/PhysRevLett.106.115303)

26. Landau LD, Lifshitz EM. 1976 *Mechanics*, 3rd edn. Course of Theoretical Physics. Oxford, UK: Elsevier.

27. Lesieur M. 2008 *Turbulence in fluids*. Dordrecht: Springer-Verlag.

28. Dar G, Verma MK, Eswaran V. 2001 Energy transfer in two-dimensional magnetohydrodynamic turbulence: formalism and numerical results. *Physica D* **157**, 207–225. (doi:10.1016/S0167-2789(01)00307-4)

29. Verma MK. 2004 Statistical theory of magnetohydrodynamic turbulence: recent results. *Phys. Rep.* **401**, 229–380. (doi:10.1016/j.physrep.2004.07.007)

30. Verma MK. 2019 *Energy transfers in fluid flows: multiscale and spectral perspectives*. Cambridge, UK: Cambridge University Press.

31. Verma MK, Chatterjee AG, Yadav RK, Paul S, Chandra M, Samtaney R. 2013 Benchmarking and scaling studies of pseudospectral code Tarang for turbulence simulations. *Pramana-J. Phys.* **81**, 617–629. (doi:10.1007/s12043-013-0594-4)

32. Chatterjee AG, Verma MK, Kumar A, Samtaney R, Hadri B, Khurram R. 2018 Scaling of a Fast Fourier Transform and a pseudo-spectral fluid solver up to 196 608 cores. *J. Parallel Distrib. Comput.* **113**, 77–91. (doi:10.1016/j.jpdc.2017.10.014)

33. Prigogine I, Stengers I. 1984 *Order out of chaos: Man's new dialogue with nature*. New York, NY: Bantam Books.

34. Prigogine I. 1962 *Non-equilibrium statistical mechanics*. New York, NY: Interscience.

35. Dallas V, Fauve S, Alexakis A. 2015 Statistical equilibria of large scales in dissipative hydrodynamic turbulence. *Phys. Rev. Lett.* **115**, 204501. (doi:10.1103/PhysRevLett.115.204501)

36. Alexakis A, Biferale L. 2018 Cascades and transitions in turbulent flows. *Phys. Rep.* **767-769**, 1–101. (doi:10.1016/j.physrep.2018.08.001)

37. Kolmogorov AN. 1941 Dissipation of energy in locally isotropic turbulence. *Dokl. Acad. Nauk. SSSR* **32**, 16–18.

38. Taylor GI. 1954 The dispersion of matter in turbulent flow through a pipe. *Proc. R. Soc. A* **223**, 446–468. (doi:10.1098/rspa.1954.0130)

39. Falkovich G, Sreenivasan KR. 2006 Lessons from hydrodynamic turbulence. *Phys. Today* **59**, 43–49. (doi:10.1063/1.2207037)

40. Verma MK. 2019 Asymmetric energy transfers in driven nonequilibrium systems and arrow of time. *Eur. Phys. J. B* **92**, 190. (doi:10.1140/epjb/e2019-100171-5)

41. Jucha J, Xu H, Pumir A. 2014 Time-reversal-symmetry breaking in turbulence. *Phys. Rev. Lett.* **113**, 054501. (doi:10.1103/PhysRevLett.113.054501)

42. Bhatnagar A, Gupta A, Mitra D, Pandit R. 2018 Heavy inertial particles in turbulent flows gain energy slowly but lose it rapidly. *Phys. Rev. E* **97**, 033102. (doi:10.1103/PhysRevE.97.033102)

43. Maity P, Govindarajan R, Ray SS. 2019 Statistics of Lagrangian trajectories in a rotating turbulent flow. *Phys. Rev. E* **100**, 043110. (doi:10.1103/PhysRevE.100.043110)

44. Pao YH. 1965 Structure of turbulent velocity and scalar fields at large wavenumbers. *Phys. Fluids* **8**, 1063–1075. (doi:10.1063/1.1761356)

45. Verma MK, Kumar A, Kumar P, Barman S, Chatterjee AG, Samtaney R, Stepanov R. 2018 Energy spectra and fluxes in dissipation range of turbulent and laminar flows. *Fluid Dyn.* **53**, 728–739. (doi:10.1134/S0015462818050166)

46. Boyd JP. 2003 *Chebyshev and fourier spectral methods*, 2nd revised edn. New York, NY: Dover Publications.

47. Ansumali S, Arcidiacono S, Chikatamarla SS, Prasianakis NI, Gorban AN, Karlin IV. 2007 Quasi-equilibrium lattice Boltzmann method. *Eur. Phys. J. B* **56**, 135–139. (doi:10.1140/epjb/e2007-00100-1)

48. Singh SK, Thantanapally C, Ansumali S. 2016 Gaseous microflow modeling using the Fokker-Planck equation. *Phys. Rev. E* **94**, 063307. (doi:10.1103/PhysRevE.94.063307)

49. Yakhot V, Orszag SA. 1986 Renormalization group analysis of turbulence. I. Basic theory. *J. Sci. Comput.* **1**, 3–51. (doi:10.1007/BF01061452)

50. Amit DJ. 1978 *Field theory, the renormalization group, and critical phenomena*. International Series in Pure and Applied Physics. Singapore: World Scientific.

51. Wilson KG, Kogut J. 1974 The renormalization group and the ε expansion. *Phys. Rep.* **12**, 75–199. (doi:10.1016/0370-1573(74)90023-4)

52. Verma MK. 2019 Description of nature: a single law or many laws? In *Indian Academy of Sciences Conference Series*, vol. 2:1, pp. 121–124.

53. Verma MK. 2019 Microscopic laws vs. macroscopic laws: perspectives from kinetic theory and hydrodynamics. (http://arxiv.org/1904.12044).

13

royalsocietypublishing.org/journal/rsta   *Phil. Trans. R. Soc. A* **378**: 20190470